Analysis of the Numerical Dispersion of the 2-D Alternating-Direction Implicit FDTD Method

An Ping Zhao, *Senior Member, IEEE*

***Abstract*—In this paper, the numerical dispersion property of the two-dimensional alternating-direction implicit finite-difference time-domain (2-D ADI FDTD) method is studied. First, we notice that the original 2-D ADI FDTD method can be divided into two sub-ADI FDTD methods: either the x-directional 2-D ADI FDTD method or the y-directional 2-D ADI FDTD method; and secondly, the numerical dispersion relations are derived for both the ADI FDTD methods. Finally, the numerical dispersion errors caused by the two ADI FDTD methods are investigated. Numerical results indicate that the numerical dispersion error of the ADI FDTD methods depends highly on the selected time step and the shape and mesh resolution of the unit cell. It is also found that, to ensure the numerical dispersion error within certain accuracy, the maximum time steps allowed to be used in the two ADI FDTD methods are different and they can be numerically determined.**

***Index Terms*—ADI FDTD method, dispersion relation, FDTD method, numerical dispersion.**

I. Introduction

In THE conventional finite-difference time-domain (FDTD) method, the time step allowed to be used is bounded by the Courant–Friedrich–Levy (CFL) stability condition. Such a condition certainly limits the capability of the traditional FDTD method, particularly when applied to problems where a very fine mesh is needed over large geometric areas. To overcome the above drawback, an interesting extension of the conventional two-dimensional (2-D) FDTD method was recently proposed by Namiki [1]. This new method was named as the 2–D alternating-direction implicit finite-difference time-domain (2–D ADI FDTD) method, which is extremely attractive because, compared with the standard FDTD algorithm, the ADI FDTD method is unconditionally stable and, thus, the CFL stability condition can be eliminated. Although the efficiency and accuracy of this new method were demonstrated [1], [2] under certain circumstances, to have a full evaluation on its performance (in terms of numerical dispersion or phase velocity), the numerical dispersion error induced by the method must be studied, and this can be done by solving the corresponding numerical dispersion relation. However, it is found that the numerical dispersion relation given in [1] was derived under some assumptions and, thus, it is inaccurate. Therefore, it is essential to find more accurate numerical dispersion relation before the performance of the ADI FDTD method is evaluated. On the other hand, it is also necessary to know how big the time step can be selected for the ADI FDTD method while the numerical dispersion error of the method is kept with certain accuracy.

In this paper, by revisiting the principle of the ADI FDTD method, we find that the original 2-D ADI FDTD method can be divided into two sub-ADI FDTD methods due to the special updating procedure used in the method. These two sub-ADI FDTD approaches can especially be named as the x-directional 2-D ADI FDTD method and the y-directional 2-D ADI FDTD method (see Section II for details), which also have different numerical dispersion relations. The numerical dispersion relations for the two 2-D ADI FDTD methods are derived. With the numerical dispersion relations given in this paper, the numerical dispersion errors caused by the ADI FDTD methods are investigated and the performances of the two ADI FDTD methods are evaluated. Numerical results indicate that the numerical dispersion errors induced by the ADI FDTD methods are strongly affected by the selected time step and the shape and mesh resolution of the unit cell. Consequently, it is revealed that, to keep the dispersion error with certain accuracy, the maximum (i.e., up limit) time steps allowed to be used in the ADI FDTD methods exist and they can be determined numerically. Empirical formulas that can be used to simply and quickly determine the maximum time steps for both the x- and y-directional 2-D ADI FDTD methods are particularly given separately for different cases.

This paper is organized as follows. In Section II, the dispersion relations for both the x- and y-directional 2-D ADI FDTD methods are derived. The numerical dispersion errors caused by the two ADI FDTD methods are comprehensively studied in Section III and, finally, conclusions and discussions are made in Section IV.

II. Derivation of the Dispersion Relations for the Two 2-D ADI FDTD Methods

As an example, we consider the 2-D TE wave. Maxwell's equation for the TE wave in an isotropic loss-free medium is [3]

$$\frac{\partial E_x}{\partial t} = \frac{1}{\varepsilon}\frac{\partial H_z}{\partial y} \tag{1a}$$

$$\frac{\partial E_y}{\partial t} = -\frac{1}{\varepsilon}\frac{\partial H_z}{\partial x} \tag{1b}$$

$$\frac{\partial H_z}{\partial t} = \frac{1}{\mu}\left(\frac{\partial E_x}{\partial y} - \frac{\partial E_y}{\partial x}\right) \tag{1c}$$

where ε and μ are the permittivity and permeability of the medium, respectively.

Manuscript received February 18, 2001; revised April 18, 2001.

The author is with the Electronics Laboratory, Nokia Research Centre, FIN-00180 Helsinki, Finland (e-mail: an-ping.zhao@nokia.com).

Publisher Item Identifier S 0018-9480(02)03030-2.

Denote any component of the fields $F_\alpha(t,x,y)$ in a discrete space as

$$F_\alpha^n(i,j) = F_\alpha(n\Delta t, i\Delta x, j\Delta y) \tag{2}$$

where $\alpha = x$ or y, n is time and i and j are space indexes, Δt is the time step, and Δx and Δy are the spatial increments along the x- and y-directions, respectively.

According to the principle of the ADI FDTD method [1], the FDTD solution marching from the nth time step to the $(n+1)$th time step is broken into two sub-updating procedures: the first updating procedure involves the advancement from the nth time step to the $(n+1/2)$th time step, whereas in the second updating procedure, the fields are advanced from the $(n+1/2)$th time step to the $(n+1)$th time step. Since in the ADI FDTD method all the field components are defined at n $(n+1/2)$ and $(n+1)$, time steps and two sub-updating procedures are involved, therefore, we have two different ways to accomplish the first and second updating procedures for the field components. Here, we use the E_x-field component as an example to explain why we have two different ways or cases: 1) $E_x^{n+1/2}$ can be updated from (E_x^n, H_z^n) in the first updating procedure, whereas E_x^{n+1} is updated from $(E_x^{n+1/2}, H_z^{n+1})$ in the second updating procedure and 2) $E_x^{n+1/2}$ is updated from $(E_x^n, H_z^{n+1/2})$ in the first updating procedure, while E_x^{n+1} is updated from $(E_x^{n+1/2}, H_z^{n+1/2})$. Therefore, in the first case, $E_x^{n+1/2}$ can be updated directly and E_x^{n+1} cannot, but in the second case, $E_x^{n+1/2}$ cannot be directly updated and E_x^{n+1} can. Due to the above reason, the above two cases should be considered separately. We define the first case as the x-directional 2-D ADI FDTD method and the second case as the y-directional 2-D ADI FDTD method. It should be noted that, according to our definition, the approach used in [1] belongs to the x-directional 2-D ADI FDTD method. In what follows, the numerical dispersion relations for the two ADI FDTD methods will be derived separately.

A. x-Directional 2-D ADI FDTD Method

For the x-directional ADI FDTD method, the two sub-updating procedures are shown in (3a)–(4c) at the bottom of the following page [1]. Equations (3) and (4) are, respectively, for the first and second updating procedures of the x-direction ADI FDTD method.

The trial solution of the fields for the TE wave is [3]

$$\begin{aligned} E_x^n(I,J) &= E_{x_0} e^{j(\omega n\Delta t - k_x I\Delta x - k_y J\Delta y)} \\ &= E_x^n e^{-j(k_x I\Delta x + k_y J\Delta y)} \end{aligned} \tag{5a}$$

$$\begin{aligned} E_y^n(I,J) &= E_{y_0} e^{j(\omega n\Delta t - k_x I\Delta x - k_y J\Delta y)} \\ &= E_y^n e^{-j(k_x I\Delta x + k_y J\Delta y)} \end{aligned} \tag{5b}$$

$$\begin{aligned} H_z^n(I,J) &= H_{z_0} e^{j(\omega n\Delta t - k_x I\Delta x - k_y J\Delta y)} \\ &= H_z^n e^{-j(k_x I\Delta x + k_y J\Delta y)} \end{aligned} \tag{5c}$$

where I and J are the space indexes and n is the time index, k_x and k_y are, respectively, the numerical wavenumbers in the x- and y-directions, and ω is the wave angle frequency.

Substituting (5) separately into (3a)–(3c) (i.e., the first updating procedure), one has

$$\begin{aligned} &\left(e^{j(\omega\Delta t)/2} - 1\right) E_x^n \\ &\quad = -j\left(\frac{\Delta t}{\varepsilon\Delta y}\right) \sin\left(\frac{k_y\Delta y}{2}\right) H_z^n \end{aligned} \tag{6a}$$

$$\begin{aligned} &\left(e^{j(\omega\Delta t)/2} - 1\right) E_y^n \\ &\quad = j\left(\frac{\Delta t}{\varepsilon\Delta x}\right) \sin\left(\frac{k_x\Delta x}{2}\right) e^{j(\omega\Delta t)/2} H_z^n \end{aligned} \tag{6b}$$

$$\begin{aligned} &\left(e^{j(\omega\Delta t)/2} - 1\right) H_z^n \\ &\quad = -j\left(\frac{\Delta t}{\mu\Delta y}\right) \sin\left(\frac{k_y\Delta y}{2}\right) E_x^n + j\left(\frac{\Delta t}{\mu\Delta x}\right) \\ &\qquad \cdot \sin\left(\frac{k_x\Delta x}{2}\right) e^{j(\omega\Delta t)/2} E_y^n \end{aligned} \tag{6c}$$

whereas substituting (5) separately into (4a)–(4c) (i.e., the second updating procedure), one obtains

$$\begin{aligned} &\left(e^{j\omega\Delta t} - e^{j(\omega\Delta t)/2}\right) E_x^n \\ &\quad = -j\left(\frac{\Delta t}{\varepsilon\Delta y}\right) \sin\left(\frac{k_y\Delta y}{2}\right) e^{j\omega\Delta t} H_z^n \end{aligned} \tag{7a}$$

$$\begin{aligned} &\left(e^{j\omega\Delta t} - e^{j(\omega\Delta t)/2}\right) E_y^n \\ &\quad = j\left(\frac{\Delta t}{\varepsilon\Delta x}\right) \sin\left(\frac{k_x\Delta x}{2}\right) e^{j(\omega\Delta t)/2} H_z^n \end{aligned} \tag{7b}$$

$$\begin{aligned} &\left(e^{j\omega\Delta t} - e^{j(\omega\Delta t)/2}\right) H_z^n \\ &\quad = -j\left(\frac{\Delta t}{\mu\Delta y}\right) \sin\left(\frac{k_y\Delta y}{2}\right) e^{j\omega\Delta t} E_x^n \\ &\qquad + j\left(\frac{\Delta t}{\mu\Delta x}\right) \sin\left(\frac{k_x\Delta x}{2}\right) e^{j(\omega\Delta t)/2} E_y^n \end{aligned} \tag{7c}$$

where $j = \sqrt{-1}$. Combining (6a) and (7a), (6b) and (7b), as well as (6c) and (7c), respectively, yields the following relations for E_x^n, E_y^n, and H_z^n:

$$\begin{aligned} &\left(e^{j\omega\Delta t} - 1\right) E_x^n \\ &\quad = -j\left(\frac{\Delta t}{\varepsilon\Delta y}\right) \sin\left(\frac{k_y\Delta y}{2}\right) \left(e^{j\omega\Delta t} + 1\right) H_z^n \end{aligned} \tag{8a}$$

$$\begin{aligned} &\left(e^{j\omega\Delta t} - 1\right) E_y^n \\ &\quad = 2j\left(\frac{\Delta t}{\varepsilon\Delta x}\right) \sin\left(\frac{k_x\Delta x}{2}\right) e^{j(\omega\Delta t)/2} H_z^n \end{aligned} \tag{8b}$$

$$\begin{aligned} &\left(e^{j\omega\Delta t} - 1\right) H_z^n \\ &\quad = -j\left(\frac{\Delta t}{\mu\Delta y}\right) \sin\left(\frac{k_y\Delta y}{2}\right) \left(e^{j\omega\Delta t} + 1\right) E_x^n + 2j\left(\frac{\Delta t}{\mu\Delta x}\right) \\ &\qquad \cdot \sin\left(\frac{k_x\Delta x}{2}\right) e^{j(\omega\Delta t)/2} E_y^n. \end{aligned} \tag{8c}$$

Equation (8) can be simplified as

$$\sin\left(\frac{\omega\Delta t}{2}\right) E_x^n = -\left(\frac{\Delta t}{\varepsilon\Delta y}\right) \sin\left(\frac{k_y\Delta y}{2}\right) \cos\left(\frac{\omega\Delta t}{2}\right) H_z^n \tag{9a}$$

$$\sin\left(\frac{\omega\Delta t}{2}\right) E_y^n = \left(\frac{\Delta t}{\varepsilon\Delta x}\right) \sin\left(\frac{k_x\Delta x}{2}\right) H_z^n \tag{9b}$$

$$\sin\left(\frac{\omega\Delta t}{2}\right)H_z^n = -\left(\frac{\Delta t}{\mu\Delta y}\right)\sin\left(\frac{k_y\Delta y}{2}\right)\cos\left(\frac{\omega\Delta t}{2}\right)\cdot E_x^n + \left(\frac{\Delta t}{\mu\Delta x}\right)\sin\left(\frac{k_x\Delta x}{2}\right)E_y^n. \quad (9c)$$

By denoting the field vector in the spatial spectral domain at the nth time step as

$$\mathbf{X}^n = \begin{bmatrix} E_x^n \\ E_y^n \\ H_z^n \end{bmatrix} \quad (10)$$

(10) can be written in a matrix form as

$$\mathbf{\Lambda X}^n = \mathbf{0} \quad (11)$$

and $\mathbf{\Lambda}$, shown in (12) at the bottom of the following page. The numerical dispersion relation is found by setting the determinant of the matrix $\mathbf{\Lambda}$ equal to zero. After some manipulation, this yields

$$\frac{1}{(\Delta x)^2}\sin^2\left(\frac{k_x\Delta x}{2}\right) + \cos^2\left(\frac{\omega\Delta t}{2}\right)\frac{1}{(\Delta y)^2}\sin^2\left(\frac{k_y\Delta y}{2}\right) = \frac{1}{(c\Delta t)^2}\sin^2\left(\frac{\omega\Delta t}{2}\right) \quad (13)$$

where $c = 1/\sqrt{\varepsilon\mu}$ is the speed of light in the medium. Equation (13) is the numerical dispersion relation for the TE wave of the x-directional ADI FDTD method. With the derivation procedure similar to the above, one can prove that (13) is also the numerical dispersion relation for the TM wave.

B. y-Directional 2-D ADI FDTD Method

For the y-directional ADI FDTD method, the two sub-updating procedures are shown in (14a)–(15c) at the bottom of the following page. Equations (14) and (15) are, respectively, for the first and second updating procedures of the y-directional ADI FDTD method. With the derivation procedure similar to

$$\frac{E_x^{n+1/2}\left(i+\frac{1}{2},j\right) - E_x^n\left(i+\frac{1}{2},j\right)}{\frac{\Delta t}{2}} = \frac{1}{\varepsilon}\left[\frac{H_z^n\left(i+\frac{1}{2},j+\frac{1}{2}\right) - H_z^n\left(i+\frac{1}{2},j-\frac{1}{2}\right)}{\Delta y}\right] \quad (3a)$$

$$\frac{E_y^{n+1/2}\left(i,j+\frac{1}{2}\right) - E_y^n\left(i,j+\frac{1}{2}\right)}{\frac{\Delta t}{2}} = -\frac{1}{\varepsilon}\left[\frac{H_z^{n+1/2}\left(i+\frac{1}{2},j+\frac{1}{2}\right) - H_z^{n+1/2}\left(i-\frac{1}{2},j+\frac{1}{2}\right)}{\Delta x}\right] \quad (3b)$$

$$\frac{H_z^{n+1/2}\left(i+\frac{1}{2},j+\frac{1}{2}\right) - H_z^n\left(i+\frac{1}{2},j+\frac{1}{2}\right)}{\frac{\Delta t}{2}} = \frac{1}{\mu}\left[\frac{E_x^n\left(i+\frac{1}{2},j+1\right) - E_x^n\left(i+\frac{1}{2},j\right)}{\Delta y} - \frac{E_y^{n+1/2}\left(i+1,j+\frac{1}{2}\right) - E_y^{n+1/2}\left(i,j+\frac{1}{2}\right)}{\Delta x}\right] \quad (3c)$$

$$\frac{E_x^{n+1}\left(i+\frac{1}{2},j\right) - E_x^{n+1/2}\left(i+\frac{1}{2},j\right)}{\frac{\Delta t}{2}} = \frac{1}{\varepsilon}\left[\frac{H_z^{n+1}\left(i+\frac{1}{2},j+\frac{1}{2}\right) - H_z^{n+1}\left(i+\frac{1}{2},j-\frac{1}{2}\right)}{\Delta y}\right] \quad (4a)$$

$$\frac{E_y^{n+1}\left(i,j+\frac{1}{2}\right) - E_y^{n+1/2}\left(i,j+\frac{1}{2}\right)}{\frac{\Delta t}{2}} = -\frac{1}{\varepsilon}\left[\frac{H_z^{n+1/2}\left(i+\frac{1}{2},j+\frac{1}{2}\right) - H_z^{n+1/2}\left(i-\frac{1}{2},j+\frac{1}{2}\right)}{\Delta x}\right] \quad (4b)$$

$$\frac{H_z^{n+1}\left(i+\frac{1}{2},j+\frac{1}{2}\right) - H_z^{n+1/2}\left(i+\frac{1}{2},j+\frac{1}{2}\right)}{\frac{\Delta t}{2}} = \frac{1}{\mu}\left[\frac{E_x^{n+1}\left(i+\frac{1}{2},j+1\right) - E_x^{n+1}\left(i+\frac{1}{2},j\right)}{\Delta y} - \frac{E_y^{n+1/2}\left(i+1,j+\frac{1}{2}\right) - E_y^{n+1/2}\left(i,j+\frac{1}{2}\right)}{\Delta x}\right] \quad (4c)$$

that used for the x-directional ADI FDTD method, one can obtain the numerical dispersion relation for both the TE and TM waves of the y-directional ADI FDTD method as

$$\cos^2\left(\frac{\omega\Delta t}{2}\right)\frac{1}{(\Delta x)^2}\sin^2\left(\frac{k_x\Delta x}{2}\right)+\frac{1}{(\Delta y)^2}\sin^2\left(\frac{k_y\Delta y}{2}\right)=\frac{1}{(c\Delta t)^2}\sin^2\left(\frac{\omega\Delta t}{2}\right). \quad (16)$$

On the other hand, it was proven [3] that the numerical dispersion relation of the standard 2-D FDTD method is

$$\frac{1}{(\Delta x)^2}\sin^2\left(\frac{k_x\Delta x}{2}\right)+\frac{1}{(\Delta y)^2}\sin^2\left(\frac{k_y\Delta y}{2}\right)=\frac{1}{(c\Delta t)^2}\sin^2\left(\frac{\omega\Delta t}{2}\right). \quad (17)$$

Comparing the numerical dispersion relations [i.e., (13) and (16)] of the 2-D ADI FDTD methods with that [i.e., (17)]

$$\mathbf{\Lambda}=\begin{bmatrix} \sin\left(\frac{\omega\Delta t}{2}\right) & 0 & \left(\frac{\Delta t}{\varepsilon\Delta y}\right)\sin\left(\frac{k_y\Delta y}{2}\right)\cos\left(\frac{\omega\Delta t}{2}\right) \\ 0 & \sin\left(\frac{\omega\Delta t}{2}\right) & -\left(\frac{\Delta t}{\varepsilon\Delta x}\right)\sin\left(\frac{k_x\Delta x}{2}\right) \\ \left(\frac{\Delta t}{\mu\Delta y}\right)\sin\left(\frac{k_y\Delta y}{2}\right)\cos\left(\frac{\omega\Delta t}{2}\right) & -\left(\frac{\Delta t}{\mu\Delta x}\right)\sin\left(\frac{k_x\Delta x}{2}\right) & \sin\left(\frac{\omega\Delta t}{2}\right) \end{bmatrix} \quad (12)$$

$$\frac{E_x^{n+1/2}\left(i+\frac{1}{2},j\right)-E_x^{n}\left(i+\frac{1}{2},j\right)}{\frac{\Delta t}{2}}=\frac{1}{\varepsilon}\left[\frac{H_z^{n+1/2}\left(i+\frac{1}{2},j+\frac{1}{2}\right)-H_z^{n+1/2}\left(i+\frac{1}{2},j-\frac{1}{2}\right)}{\Delta y}\right] \quad (14a)$$

$$\frac{E_y^{n+1/2}\left(i,j+\frac{1}{2}\right)-E_y^{n}\left(i,j+\frac{1}{2}\right)}{\frac{\Delta t}{2}}=-\frac{1}{\varepsilon}\left[\frac{H_z^{n}\left(i+\frac{1}{2},j+\frac{1}{2}\right)-H_z^{n}\left(i-\frac{1}{2},j+\frac{1}{2}\right)}{\Delta x}\right] \quad (14b)$$

$$\frac{H_z^{n+1/2}\left(i+\frac{1}{2},j+\frac{1}{2}\right)-H_z^{n}\left(i+\frac{1}{2},j+\frac{1}{2}\right)}{\frac{\Delta t}{2}}=\frac{1}{\mu}\left[\frac{E_x^{n+1/2}\left(i+\frac{1}{2},j+1\right)-E_x^{n+1/2}\left(i+\frac{1}{2},j\right)}{\Delta y}-\frac{E_y^{n}\left(i+1,j+\frac{1}{2}\right)-E_y^{n}\left(i,j+\frac{1}{2}\right)}{\Delta x}\right] \quad (14c)$$

$$\frac{E_x^{n+1}\left(i+\frac{1}{2},j\right)-E_x^{n+1/2}\left(i+\frac{1}{2},j\right)}{\frac{\Delta t}{2}}=\frac{1}{\varepsilon}\left[\frac{H_z^{n+1/2}\left(i+\frac{1}{2},j+\frac{1}{2}\right)-H_z^{n+1/2}\left(i+\frac{1}{2},j-\frac{1}{2}\right)}{\Delta y}\right] \quad (15a)$$

$$\frac{E_y^{n+1}\left(i,j+\frac{1}{2}\right)-E_y^{n+1/2}\left(i,j+\frac{1}{2}\right)}{\frac{\Delta t}{2}}=-\frac{1}{\varepsilon}\left[\frac{H_z^{n+1}\left(i+\frac{1}{2},j+\frac{1}{2}\right)-H_z^{n+1}\left(i-\frac{1}{2},j+\frac{1}{2}\right)}{\Delta x}\right] \quad (15b)$$

$$\frac{H_z^{n+1}\left(i+\frac{1}{2},j+\frac{1}{2}\right)-H_z^{n+1/2}\left(i+\frac{1}{2},j+\frac{1}{2}\right)}{\frac{\Delta t}{2}}=\frac{1}{\mu}\left[\frac{E_x^{n+1/2}\left(i+\frac{1}{2},j+1\right)-E_x^{n+1/2}\left(i+\frac{1}{2},j\right)}{\Delta y}-\frac{E_y^{n+1}\left(i+1,j+\frac{1}{2}\right)-E_y^{n+1}\left(i,j+\frac{1}{2}\right)}{\Delta x}\right] \quad (15c)$$

of the standard 2-D FDTD method, one can easily notice the difference between them: in (13), one extra term, i.e., $\cos^2(\omega\Delta t/2)$, imposes on the wavenumber k_y, whereas in (16), the extra term imposes on the wavenumber k_x. In other words, the wavenumber k_x in (13) is "unaffected" (this is why we named it as the x-directional 2-D ADI FDTD method), and the wavenumber k_y in (16) is "uninfluenced" (this is why we called it the y-directional 2-D ADI FDTD method). However, it should be pointed out here that dividing the original 2-D ADI FDTD method into the above two different approaches (i.e., the x- and y-directional 2-D ADI FDTD methods) is also motivated by the two different three-dimensional (3-D) ADI FDTD algorithms [4], [5]. For example, the x-directional 2-D ADI FDTD method can be directly reduced from the 3-D ADI FDTD algorithm [5] and the y-directional 2-D ADI FDTD method can be directly derived from the 3-D ADI FDTD approach [4]. Nevertheless, it should be noted that the 3-D ADI FDTD approaches [4], [5] cannot be simply defined as either the x-directional or y-directional 3-D ADI FDTD method, as in the 3-D case, one more direction (i.e., the z-direction) is involved in the updating equations.

It is apparent that when Δt, Δx, and Δy all go to zero, the numerical dispersion relations [i.e., (13) and (16)] of the two 2-D ADI FDTD methods will convert to the theoretical dispersion relation

$$k_x^2 + k_y^2 = \frac{\omega^2}{c^2} = k^2 \tag{18}$$

where $k = (\omega/c)$ is the theoretical wavenumber.

The numerical dispersion relation given in [1] (note: there is also a printing error in [1, eq. (19)]) is

$$\frac{1}{(\Delta x)^2}\sin^2\left(\frac{k_x\Delta x}{2}\right) + \frac{1}{(\Delta y)^2}\sin^2\left(\frac{k_y\Delta y}{2}\right) = \frac{4}{(c\Delta t)^2}\sin^2\left(\frac{\omega\Delta t}{4}\right)\cos^{-1}\left(\frac{\omega\Delta t}{2}\right). \tag{19}$$

As explained earlier, the ADI FDTD algorithm used in [1] belongs to the x-directional 2-D ADI FDTD method. This also means that (19) relates to the numerical dispersion relation of the x-directional ADI FDTD method and, thus, (13) and (19) can be compared. By comparing (13) with (19), one can easily notice the significant difference between them. However, it should be noticed that (19) was derived under the assumption that the growth factors of the first and second updating procedures are always identical (i.e., $\xi_1 = \xi_2$, see [1] for details). On the other hand, the correctness of the expressions used for E_x, E_y and H_z (see [1, eqs. (7) and (8)]) in [1] is questionable. However, the trial solutions of E_x, E_y, and H_z [i.e., (5)] used in this paper are suitable for all kinds of FDTD methods [3]. This is why we claimed that the numerical dispersion relations of the 2-D ADI FDTD methods derived in this paper are more accurate and reasonable than the one given in [1].

III. Numerical Dispersion Properties of the ADI FDTD Methods

The numerical dispersion characteristics of the ADI FDTD methods can be studied by solving the dispersion relations given in (13) and (16). To solve (13) and (16), let us assume that wave propagates at an angle θ with respect to the positive x-direction (i.e., $k_x = k\cos\theta$ and $k_y = k\sin\theta$), thus the numerical solution of the wavenumber k can be easily obtained with the Newton's iteration method for a given set of parameters Δx, Δy, Δt, and θ. Particularly, for the x-directional ADI FDTD method, (13) can be solved for the numerical wavenumber k at any wave propagation angle θ as

$$k_{i+1} = k_i - \frac{\dfrac{\sin^2(Ak_i)}{(\Delta x)^2} + \cos^2\left(\dfrac{\omega\Delta t}{2}\right)\dfrac{\sin^2(Bk_i)}{(\Delta y)^2} - C}{\dfrac{A\sin(2Ak_i)}{(\Delta x)^2} + \cos^2\left(\dfrac{\omega\Delta t}{2}\right)\dfrac{B\sin(2Bk_i)}{(\Delta y)^2}} \tag{20}$$

whereas for the y-directional ADI FDTD method, (16) can be solved for the numerical wavenumber k at any wave propagation angle θ as

$$k_{i+1} = k_i - \frac{\cos^2\left(\dfrac{\omega\Delta t}{2}\right)\dfrac{\sin^2(Ak_i)}{(\Delta x)^2} + \dfrac{\sin^2(Bk_i)}{(\Delta y)^2} - C}{\cos^2\left(\dfrac{\omega\Delta t}{2}\right)\dfrac{A\sin(2Ak_i)}{(\Delta x)^2} + \dfrac{B\sin(2Bk_i)}{(\Delta y)^2}}. \tag{21}$$

In addition, to evaluate the performances of the ADI FDTD methods, it is also necessary to compare them with the numerical dispersion property of the conventional 2-D FDTD method, and the numerical wavenumber k for the conventional 2-D FDTD method can be solved with [3]

$$k_{i+1} = k_i - \frac{\dfrac{\sin^2(Ak_i)}{(\Delta x)^2} + \dfrac{\sin^2(Bk_i)}{(\Delta y)^2} - C}{\dfrac{A\sin(2Ak_i)}{(\Delta x)^2} + \dfrac{B\sin(2Bk_i)}{(\Delta y)^2}} \tag{22}$$

where k_{i+1} is the improved estimate of k_i, k_i is the previous estimate of k, and the coefficients A, B, and C used in (20)–(22) are defined as

$$\begin{aligned} A &= \frac{\Delta x\cos\theta}{2} \\ B &= \frac{\Delta y\sin\theta}{2} \\ C &= \frac{1}{(c\Delta t)^2}\sin^2\left(\frac{\omega\Delta t}{2}\right). \end{aligned} \tag{23}$$

For (20)–(22), a very good initial guess for $k_{i=0}$ is ω/c, which is the theoretical wavenumber [as shown in (18)] of the corresponding mode in the medium [3]. Therefore, it is easily shown that the normalized numerical phase velocity v_p/c is given by

$$\frac{v_p}{c} = \frac{k}{k_{\text{final}}} = \frac{\omega}{ck_{\text{final}}} \tag{24}$$

where k_{final} is the final result of the Newton's iteration method and $k(=\omega/c)$ is, again, the theoretical wavenumber. Usually, only two or three iterations are required for convergence.

If within the entire computational region the 2-D FDTD unit cell is defined by ($\Delta x \times \Delta y$), then the time step used in the

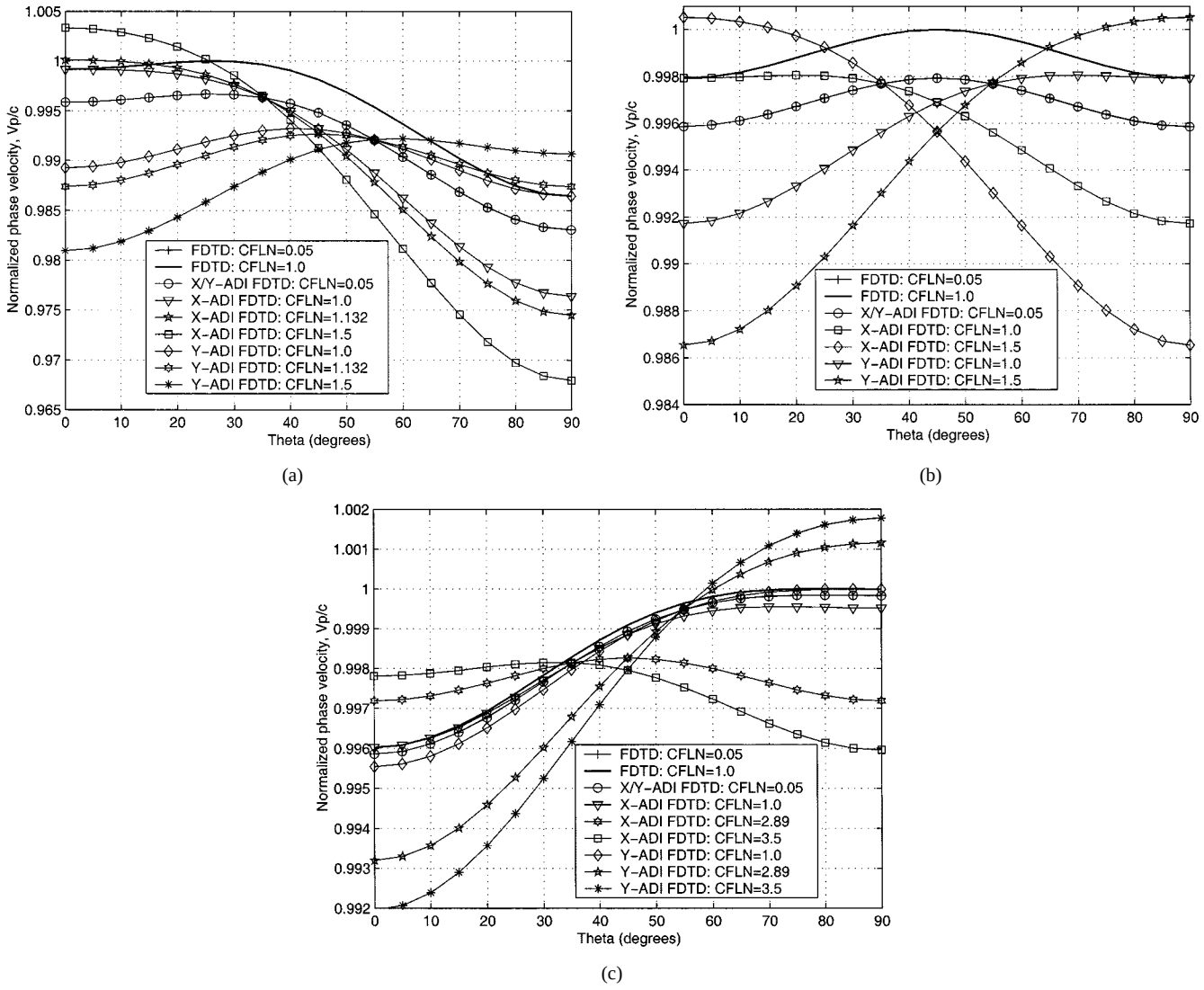

Fig. 1. Normalized phase velocity of the x- and y-directional ADI FDTD methods as functions of the CFLN. Mesh resolution is $N = 20$. (a) $R = 0.5$. (b) $R = 1.0$. (c) $R = 5.0$.

standard 2-D FDTD method is bounded by the following CFL condition [3]:

$$\Delta t \le \Delta t_{\max}^{\mathrm{FDTD}} = \frac{1}{c\sqrt{\dfrac{1}{(\Delta x)^2} + \dfrac{1}{(\Delta y)^2}}}. \tag{25}$$

To make the discussion easier, we define the ratio of $\Delta t/\Delta t_{\max}^{\mathrm{FDTD}}$ as the CFL number (CFLN), i.e., $\mathrm{CFLN} = \Delta t/\Delta t_{\max}^{\mathrm{FDTD}}$; and the shape of the 2-D FDTD unit cell is described by another ratio $R = \Delta x/\Delta y$. In addition, for the definition of the mesh resolution used in this paper, we define $\Delta x = \lambda/N$ (where λ is the operating frequency and $N \ge 10$) as the different mesh resolution of the unit cell. For example, if we have $R = 5$ and $N = 15$ for the unit cell, then the sizes of this unit cell in the x- and y-directions are $\Delta x = \lambda/15$ and $\Delta y = \Delta x/R = \lambda/75$, respectively. Moreover, if the mesh resolution is $N = 20$, then the smallest value of R is 0.5 since, to ensure the accuracy of the FDTD method, the spatial increment (either Δx or Δy) should not be greater than $\lambda/10$. Due to the same reason, the smallest value of R is 0.25 if the mesh resolution is $N = 40$.

The normalized phase velocities (i.e., v_p/c) of the x- and y-directional 2-D ADI FDTD methods for the cases $R = 0.5$, $R = 1.0$, and $R = 5.0$ (for all the cases, the mesh resolution is $N = 20$) are shown in Fig. 1(a)–(c), respectively. For comparison, the normalized phase velocities of the standard FDTD method are also plotted in Fig. 1. It can be seen from Fig. 1 that, for any values of R, the normalized phase velocities of the standard FDTD method and the two ADI FDTD methods overlap each other when the CFLN closes to zero, for instance, they are almost indistinguishable even at $\mathrm{CFLN} = 0.05$ [note: although for the case $\mathrm{CFLN} = 0.05$ the normalized phase velocities of the two ADI FDTD methods are not exactly identical, the difference between them is extremely small and, thus, only one curve is used to represent the results of both the ADI FDTD methods, as shown in Fig. 1(a)-(c)]. Since the normalized phase velocities vary very much with the angle θ, so should the performance of the FDTD methods be determined or evaluated by the maximum absolute value of $(1 - v_p/c)$ within the entire range of θ. For example, when the parameters $R = 0.5$ and $\mathrm{CFLN} = 1.5$ are used for the x-directional ADI FDTD

method, the maximum absolute value of $(1 - v_p/c)$ occurs at $\theta = 90°$, as can be seen in Fig. 1(a). With this criterion, one can see from Fig. 1 that, for any values of R, the best performance of the conventional FDTD method is reached when the value of CFLN is 1.0 and its worst performance appears when the value of CFLN closes to zero. However, for the ADI FDTD methods, the situation is more complicated and the performance is strongly influenced by the value of R (i.e., the shape of the unit cell). For example, for the case $R = 0.5$, one can see from Fig. 1(a) that the performance of the x-directional ADI FDTD method is continuously getting worse while CFLN is increased and, thus, the best performance is reached when CFLN closes to zero. However, for the y-directional ADI FDTD method, the performance gets better first and then worse while CFLN increases (from 0.05) and the best performance is reached when $\mathrm{CFLN} = 1.132$, i.e., when the profile of the normalized phase velocity is symmetric [i.e., $v_p/c(\theta) = v_p/c(90° - \theta)$] about the angle $\theta = 45°$. Therefore, for both the x- and y-directional ADI FDTD methods, we may conclude that: 1) if the performance always gets worst while CFLN increases, then the best performance is obtained when the CFLN closes to 0.0 or 2) if the performance gets better first (and then worse) when the CFLN increases, then the best performance is reached when the profile of v_p/c is symmetric about the angle $\theta = 45°$. With the above remarks for the ADI FDTD methods, one can see from Fig. 1(b) that, for the $R = 1.0$ case, the best performances of the two ADI FDTD methods are reached when the CFLN closes to zero, but for the case $R = 5.0$, the best performances of the x- and y-directional ADI FDTD methods are, respectively, reached when the CFLN equals to 2.89 and closes to 0.0, as shown in Fig. 1(c). In addition, it is interesting to note from Fig. 1 that, for R with a certain value, there are some special directions for the x- and y-directional ADI FDTD methods: the value of the normalized phase velocity of the x-directional ADI FDTD method is almost unchanged around the propagation direction $\theta = 35.5°$ even when CFLN varies; whereas for the y-directional ADI FDTD method, such a special direction is around the direction $\theta = 54.5°$. This indicates that, if one wants to use the recorded field profile to evaluate the performance (as function of the CFLN) of the ADI FDTD methods (like the manner used in [2]), then the field profile should not be recorded around these two special directions; and it is recommended to use the field profile recorded at the direction $\theta = 0°$ or $\theta = 90°$ for the evaluation, as the worst performance of both the ADI FDTD methods always appears at either the $\theta = 0°$ or $\theta = 90°$ direction.

To further demonstrate that the numerical dispersion errors caused by the ADI FDTD methods are highly influenced by the shape and mesh resolution of the unit cell as well as the value of CFLN, the maximum dispersion errors [i.e., absolute value of $(1 - v_p/c)$] of the two ADI FDTD methods are shown in Fig. 2, where the results plotted in Fig. 2(a) and (b) are for the mesh resolution $N = 20$ and $N = 40$, respectively. Note that for the results shown in Fig. 2, we consider only the $\mathrm{CFLN} \geq 1.0$ cases due to the original purpose of the ADI FDTD method. From Fig. 2, one can see that, for the $R = 1.0$ case, the performances of the two ADI FDTD methods are exactly identical. Moreover,

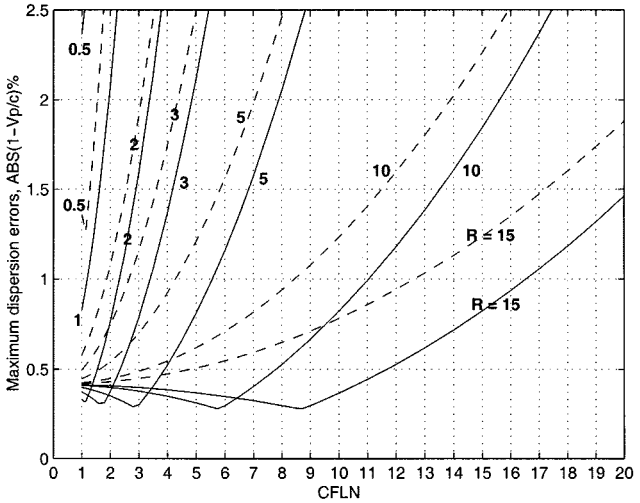

(a)

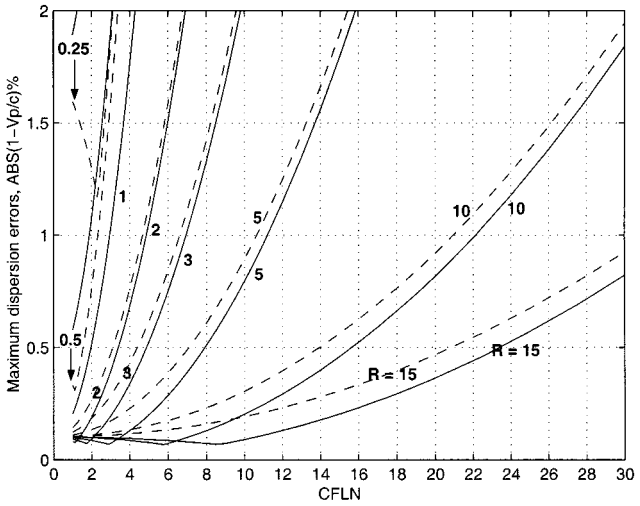

(b)

Fig. 2. Maximum dispersion errors of the x-directional ADI FDTD method (solid curves) and the y-directional ADI FDTD method (dashed curves) as functions of the CFLN and R. (a) Mesh resolution: $N = 20$. (b) Mesh resolution: $N = 40$.

for the $R < 1.0$ case, the performance of the x-directional ADI FDTD method is continuously getting worst when the CFLN is increased. However, for the y-directional ADI FDTD method, the performance is getting better first and then worse while the CFLN is increased. However, for the $R > 1.0$ case, the situation for the two ADI FDTD methods is just reversed and the best performance of the x-directional ADI FDTD method appears at $\mathrm{CFLN} \approx 0.58R$. In addition, it can also be seen from Fig. 2 that, to have a fixed accuracy, the maximum values of the CFLN allowed to be used for the ADI FDTD methods cannot exceed certain levels, which certainly indicates that an up limit for the CFLN exists.

Fig. 3(a) and (b) shows the maximum values of the CFLN (as functions of R and N) allowed to be used in the ADI FDTD methods when the required accuracy is, respectively, set to be 1.0% and 0.5%. It can be found from Fig. 3(a) and (b) that, for the $R > 1.0$ case, the maximum value of the CFLN allowed to be used in the x-directional ADI FDTD method is always greater than that of the y-directional ADI

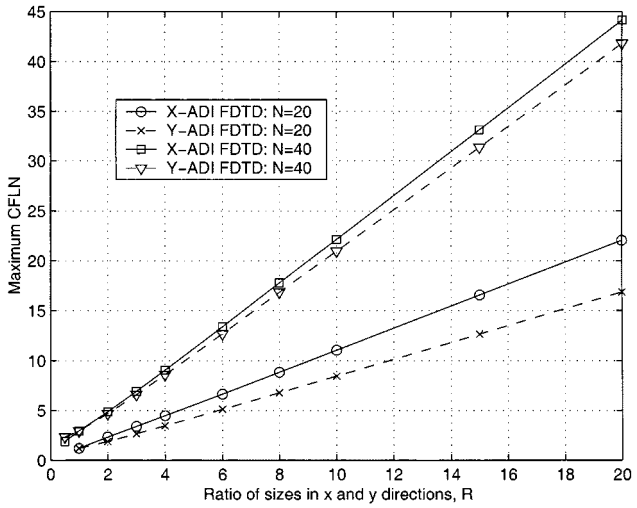

(a)

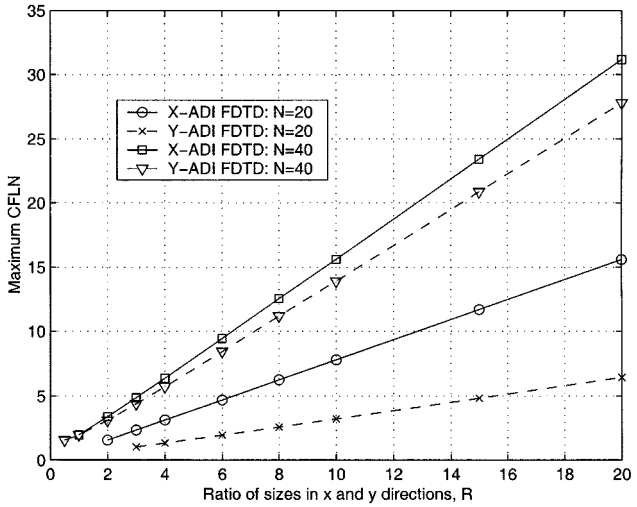

(b)

Fig. 3. Maximum CFLN allowed to be used in the x-directional ADI FDTD method (solid lines) and the y-direction ADI FDTD method (dashed lines) as functions of R and N. (a) With accuracy of 1.0%. (b) With accuracy of 0.5%.

FDTD method, and vice versa for the $R < 1.0$ case. This certainly means that, to increase the efficiency of the ADI FDTD methods, the x-directional ADI FDTD method should be used for the $R > 1.0$ case and the y-directional ADI FDTD method should be adopted for the $R < 1.0$ case. However, if for the unit cell we have $R = 1.0$, then either the x- or y-directional ADI FDTD method can be used, as they have the same performance. This implies that whether the x-directional ADI FDTD method or the y-directional ADI FDTD method should be adopted depends on how the computational space is meshed. In addition, it can also be found from Fig. 3(a) and (b) that, for the same mesh resolution, the maximum allowed value of the CFLN gets greater when R increases, and for the same value of R, the maximum allowed value of the CFLN gets bigger when the mesh resolution increases. This indicates that, compared to the standard FDTD method, the ADI FDTD method is more efficient (in terms of saving CPU time) *only* when the value of R is relatively big and/or the mesh resolution of the smallest unit cell is fairly high. Consequently, it is found from Fig. 3 that, for the x-directional ADI FDTD method, one can have the following empirical formulas to simply and quickly determine the maximum allowed values of the CFLN: the maximum values of the CFLN are, respectively, bounded by $\mathrm{CFLN} \leq (\mathrm{NR})/18.1 = (\lambda_{\min} R)/(18.1\Delta x)$ and $\mathrm{CFLN} \leq (\mathrm{NR})/25.6 = (\lambda_{\min} R)/(25.6\Delta x)$ when the required accuracy is set to be 1.0% and 0.5%. The above two formulas used for the x-directional ADI FDTD method work well for both the $N = 20$ and $N = 40$ cases. However, as can be seen from Fig. 3, for the y-directional ADI FDTD method, no such common empirical formulas can be found, which means that different empirical formulas must be used for different cases (i.e., with different required accuracies, as well as different mesh resolutions). For examples, when the required accuracy is set to be 1.0% for the y-directional ADI FDTD method, the maximum values of the CFLN for the mesh resolutions $N = 20$ and $N = 40$ are, respectively, bounded by $\mathrm{CFLN} \leq (\mathrm{NR})/23.6 = R/1.18$ and $\mathrm{CFLN} \leq (\mathrm{NR})/19.2 = R/0.48$; and while the required accuracy is set to be 0.5%, the maximum values of the CFLN are bounded by $\mathrm{CFLN} \leq (\mathrm{NR})/62 = R/3.1$ and $\mathrm{CFLN} \leq (\mathrm{NR})/28.8 = R/0.72$ for the mesh resolutions $N = 20$ and $N = 40$, respectively. Finally, it is worth mentioning that all the above empirical formulas work well only when the conditions $R \geq 1.0$ and (the predicated) $\mathrm{CFLN} \geq 1.0$ are *simultaneously* satisfied. This means that, for instance, if the required accuracy is set to be 0.5% for the y-directional ADI FDTD method with $N = 20$, then the smallest value of R allowed to be used in the empirical formula is 3.1.

IV. Conclusions and Discussions

In this paper, we first found that the original 2-D ADI FDTD method can be classified as the x-directional 2-D ADI FDTD method and the y-directional 2-D ADI FDTD method due to the special updating procedure used in the ADI FDTD technique. Consequently, more accurate and reasonable (comparing to the one presented in [1]) numerical dispersion relations for both the ADI FDTD methods were derived. With the numerical dispersion relations given in this paper, the numerical dispersion property of the 2-D ADI FDTD methods was comprehensively studied. Numerical results indicate that the numerical dispersion errors caused by the 2-D ADI FDTD methods are highly affected by the selected time step, shape, and mesh resolution of the unit cell. Moreover, it reveals that, to keep numerical results obtained with the 2-D ADI FDTD methods within certain accuracy, the up limit for the time step exists and, consequently, it can be numerically determined with the empirical formulas given in this paper. Furthermore, how the efficiency of the 2-D ADI FDTD methods can be increased is also briefly discussed. In addition, it needs to be pointed out here that the strategy used in this paper for determining the up limit of the 2-D ADI FDTD methods can also be applied to the 3-D ADI FDTD method, but for the 3-D case, one extra parameter should be adopted to describe the shape of the 3-D FDTD unit cell.

From the materials presented in this paper and elsewhere [1], [4], [6], one can easily realize that the derivation of the numerical dispersion relations and the proof of the numerical stability for the ADI FDTD method are more difficult than those for

the standard FDTD method due to the complexity of the ADI FDTD method. Thus far, two different ways for deriving the numerical dispersion relations of the ADI FDTD method have been proposed; and the main difference between these two ways is the derivation procedure is started from either the original updating equations (as used in [1] and here for the 2-D case) or the actual updating equations (as used in [6] for the 3-D case). Beginning the derivation procedure from the actual updating equations might be more reasonable than that from the original updating equations. Therefore, as the next step for the numerical dispersion analysis of the 2-D ADI FDTD methods, investigations on the derivation of the numerical dispersion relations from their actual updating equations will be carried out. Obviously, the format of the numerical dispersion relations (of the 2-D ADI FDTD methods) derived from the actual updating equations will be more complicated than the one given in this paper. However, the numerical dispersion relations derived from the above different ways might be closely related, e.g., they are convertible from one to another under certain conditions/assumptions or they provide similar results. On the other hand, the theoretical prediction on the numerical dispersion errors of the 2-D ADI FDTD methods presented in this paper needs to be validated with numerical simulations, which is also left for future work.

REFERENCES

[1] T. Namiki, "A new FDTD algorithm based on alternating direction implicit method," *IEEE Trans. Microwave Theory Tech.*, vol. 47, pp. 2003–2007, Oct. 1999.

[2] T. Namiki and K. Ito, "Investigation of the numerical errors of the two-dimensional ADI–FDTD method," *IEEE Trans. Microwave Theory Tech.*, vol. 48, pp. 1950–1956, Nov. 2000.

[3] A. Taflove, *Computational Electromagnetics—The Finite-Difference Time-Domain Method*. Norwood, MA: Artech House, 1995.

[4] F. Zheng, Z. Chen, and J. Zhang, "Toward the development of a three-dimensional unconditionally stable finite-difference time-domain method," *IEEE Trans. Microwave Theory Tech.*, vol. 48, pp. 1550–1558, Sept. 2000.

[5] T. Namiki, "3-D ADI-FDTD method—unconditionally stable time-domain algorithm for solving full vector Maxwell's equations," *IEEE Trans. Microwave Theory Tech.*, vol. 48, pp. 1743–1748, Oct. 2000.

[6] F. Zheng and Z. Chen, "Numerical dispersion analysis of the unconditionally stable 3D ADI–FDTD method," *IEEE Trans. Microwave Theory Tech.*, vol. 49, pp. 1006–1009, May 2001.

An Ping Zhao (M'97–SM'98) received the B.Sc. degree in optical physics from the Changchun Institute of Optics and Fine Mechanics, Changchun, China, in 1984, the M.Sc. degree in optics from the Changchun Institute of Physics, Chinese Academy of Sciences, Changchun, China, in 1987, and the Ph.D. degree in electronic and electrical engineering from Brunel University, Brunel, U.K., in 1994.

From 1987 to 1989, he was an Associate Researcher at the Changchun Institute of Physics. In January 1990, he joined the Department of Electronic and Electrical Engineering, Surrey University, Surrey, U.K., as a Visiting Research Fellow, where he was involved with the computer verification of optical waveguide characteristics based on multiple-quantum-well (MWQ) structures in III–V semiconductor materials. In September 1994, he joined the Department of Electrical and Communications Engineering, Radio Laboratory, Helsinki University of Technology, Helsinki, Finland, where he was involved with the computer-aided design of microwave and millimeter-wave circuits with the FDTD method. Since October 1997, he has been a Senior Research Engineer with the Electronics Laboratory, Nokia Research Centre, Helsinki, Finland. His research interests include numerical modeling of microwave and millimeter-wave circuits and antenna design for wireless communications. He is listed in *Who's Who in the World*.